JEE Journal of Ecological Engineering

Journal of Ecological Engineering, 2026, 27(3), 274–287
https://doi.org/10.12911/22998993/213631
ISSN 2299–8993, License CC-BY 4.0

Received: 2025.10.13
Accepted: 2025.11.26
Published: 2026.02.01

Theoretical framework and preliminary experimental evaluation of magnetically enhanced production of hydroxyl radicals in cavitating flows for wastewater treatment

Petr Sikora[1*], Simona Fialová[1], František Pochylý[1], Eliška Maršálková[2]

[1] Viktor Kaplan Department of Fluid Engineering, Brno University of Technology, Technická 2896/2, Brno, 616 69, Czech Republic
[2] Institute of Botany, Czech Academy of Sciences, Lidická 25/27, Brno, 602 00, Czech Republic
* Corresponding author's e-mail: Petr.Sikora1@vutbr.cz

ABSTRACT

Hydrodynamic cavitation presents a promising approach to degrading recalcitrant organic pollutants in wastewater, as it generates extreme conditions that promote the formation of reactive oxygen species, particularly hydroxyl radicals. However, cavitation alone typically does not ensure sufficient radical production for effective water treatment, and is, therefore, often coupled with other advanced oxidation processes to enhance free radical yield. Non-equilibrium thermodynamics suggests that chemical reactions in cavitating liquids can be intensified through auxiliary physical effects, such as the relatively unexplored influence of an external magnetic field. This study presents a novel theoretical framework based on phenomenological principles of irreversible thermodynamics and experimentally evaluates the suggested beneficial effect of the synergistic combination of hydrodynamic cavitation and magnetic field. Conducted chemical analyses of treated tap water indicate increased radical activity, particularly reflected in shifts in pH and oxidation-reduction potential. The study highlights the potential of integrating magnetic fields into advanced oxidation processes and demonstrates the value of non-equilibrium thermodynamics concepts in understanding and optimizing such processes.

Keywords: non-equilibrium thermodynamics, hydrodynamic cavitation, magnetic field, hydroxyl radical, wastewater treatment, advanced oxidation process.

INTRODUCTION

Hydrodynamic cavitation (HC) as a representative of advanced oxidation processes (AOPs) is currently receiving increased attention in the field of wastewater treatment. Recent studies (Lei et al., 2024; Hübner et al., 2024; Gągol et al., 2018) have shown that the synergistic combination of HC with other AOPs can successfully degrade recalcitrant organic pollutants like industrial effluents (Kanthale et al., 2023), bacteria (Marsalek et al., 2020; Abramov et al., 2021), viruses (Filipić et al., 2023), dyes (Nie et al., 2022), pesticides, or pharmaceutical compounds, such as antibiotics (Abramov et al., 2022; Patil et al., 2022; Yi et al., 2022), estrogens, and other drug residues (Dixit et al., 2023; Thanekar et al., 2020).

HC is, by itself, capable of producing free radicals necessary for the degradation of recalcitrant organic compounds (Kalmár et al., 2020; Nie et al., 2021; Peng et al., 2022). Nevertheless, its standalone treatment efficiency is generally insufficient for the effective removal of the majority of polluting substances. For this reason, cavitation is typically combined with other AOPs that further enhance radical production. The most common approach involves integrating HC or acoustic cavitation with low-temperature plasma discharge (Abramov et al., 2021, 2022; Filipić et al., 2023; Lei et al., 2024; Marsalek et al., 2020; Nie et al., 2022), followed by the use of supporting chemical additives such as Fenton's reagent (Lakshmi et al., 2021; Kanthale et al., 2023), ozone (Dixit et al., 2023; Raut-Jadhav et al., 2016; Thanekar et

al., 2020), hydrogen peroxide (Patil et al., 2022; Yi et al., 2022), and other chemicals, including their combined effect.

When examining the chronological development of research into cavitation-assisted AOPs for large-scale wastewater treatment, a clear trend emerges: low-temperature plasma discharge has gradually been established as the most effective means of intensifying free radical production initiated by cavitation. Before this consensus was reached, the scientific community conducted numerous experimental studies (Abramov et al., 2021, 2022; Filipić et al., 2023; Lei et al., 2024; Marsalek et al., 2020; Nie et al., 2022; Peng et al., 2022). They were initially focused on the individual phenomena, while their combined effect on treatment efficiency was investigated afterwards.

These experiments were conducted in an intuitive manner, without reference to the mathematical models provided by non-equilibrium thermodynamics. However, it is precisely these models from which a novel hypothesis emerges. The presented hypothesis – based on the so-called Curie–Prigogine principle (Prigogine, 1967) – states that in a non-isotropic medium, chemical reactions can be induced by the influence of fields of different physical nature. This includes, in particular, magnetic fields, whose role remains largely underexplored in the existing literature. This approach treats individual AOPs as irreversible processes contributing to entropy production in the system and examines the potential for their mutual interaction. Crucially, it offers the mathematical framework for describing the interdependence of these phenomena in enhancing the generation of chemical compounds with disinfectant properties (mainly free radicals).

The output of this study is an experimental validation of the proposed hypothesis through a comparison of chemical changes in a liquid treated by a combination of HC and an external magnetic field versus HC treatment only. Should the influence of the magnetic field prove sufficiently significant within the context of other AOPs, more targeted experimental scenarios may be investigated in future research, including the effect of the magnetic field on the concentration of specific pollutants. This effort will then allow for follow-up studies combining all three physical phenomena into a conjoint technology.

State of the art

Although research into the combination of HC with the above-mentioned AOPs is gaining increased scientific attention, the influence of an external magnetic field on a cavitating liquid has so far been explored to a lesser extent. Previous research has primarily focused on the effects of magnetic fields on water properties (Cai et al., 2009; Chang and Weng, 2006; Liu et al., 2011; Toledo et al., 2008) or cavitation dynamics (Yoshimura et al., 2022), rather than on their potential application in wastewater treatment. According to these studies, the application of a magnetic field of sufficient strength was found to prolong the lifetime of cavitation bubbles, increase their number, and slow down their collapse. At the same time, an external magnetic field strengthens hydrogen bonds in water molecules and increases conductivity and pH while decreasing surface tension. Nevertheless, the investigation of the effects of water magnetization still remains a controversial and ambiguous subject. Contradictory reports regarding the influence of magnetic fields imply that their effectiveness may be limited to specific conditions (Wang et al., 2018).

A recent study by Hordieiev et al. (2024) investigated the synergistic effect of acoustic cavitation and the magnetic ion activation effect. While cavitation aims to break hydrogen bonds in water molecules, a fluctuating magnetic field is expected to provide a supplementary supporting effect. The principle is described as disrupting the spin orientation of electrons and nuclei and reducing the energy of intermolecular interactions. To an extent, the results confirmed the presented theory, with the overall water quality shown to improve based on experimentally measured data. The time evolution of pH, oxidation-reduction potential (ORP), and total dissolved solids (TDS) was compared for samples of tap and river water, with TDS decreasing considerably in tap water and also – to a lesser extent – in river water.

Cavitation bubble dynamics

The rapid collapse of cavitation bubbles leads to extreme physical conditions, resulting in both mechanical and chemical effects, primarily the dissociation of water vapor and dissolved gases into free radicals. Hydroxyl radicals (OH•) constitute the bulk of the produced reactive oxygen species (ROS) and play a crucial role in

subsequent physicochemical reactions. High redox potential (ORP) and the non-selective nature of ROS ensure successful degradation of most organic pollutants. Other commonly formed ROS include hydrogen peroxide (H_2O_2), ozone (O_3), hydroperoxyl radicals (HO_2•), and atomic oxygen (O). According to the simulations of cavitation bubble dynamics performed by Peng et al. (2022), the pursuit of maximizing radical production is not always justified. On the contrary, excessive production may actually cause an undesirable phenomenon where hydroxyl radicals tend to accumulate within a boundary layer near the gas-liquid interface, as shown in Figure 1. In this confined region, recombination reactions can occur, leading to the formation of less reactive species such as H_2O_2, thereby diminishing the overall oxidative capacity (Kalmár et al., 2020; Nie et al., 2021; Peng et al., 2022; Satyam and Patra, 2025; Zupanc et al., 2013).

The cavitation intensity can be quantified using the dimensionless cavitation number σ (or C_v):

$$\sigma = \frac{p_1 - p_v}{p_1 - p_2} \quad (1)$$

where: p_1 and p_2 represent the inlet and outlet pressure values measured in the vicinity of the Venturi nozzle while p_v denotes the saturation vapor pressure.

The smaller the number, the easier it is for cavitation to occur in the flow field. Each experimental configuration requires its own determination of an optimal σ range. While parameters like solid particle concentration can enhance cavitation, excessive intensity may lead to bubble coalescence. In such cases, larger bubbles escape from the liquid without collapsing or suffer incomplete collapse, in turn reducing the amount of free radicals produced (Gągol et al., 2018; Lei et al., 2024; Nie et al., 2022; Peng et al., 2022; Rajoriya et al., 2016).

NON-EQUILIBRIUM THERMODYNAMICS

Unlike classical thermodynamics, non-equilibrium thermodynamics considers a thermodynamic system not as isolated (i.e., without the exchange of matter or energy with its surroundings), but rather as closed or even open, allowing for interactions in the form of mass and energy fluxes across the system boundary. When a thermodynamic system is displaced from equilibrium, often by external influences, generalized thermodynamic forces X emerge in an attempt to restore equilibrium. These forces in turn produce generalized thermodynamic fluxes J, which, through various irreversible processes, contribute to an increase in the system's entropy (de Groot and Mazur, 1984; Maršík, 1999; Prigogine, 1967).

This behavior can be described mathematically using entropy production $\mathcal{P}$, defined as a sum of N irreversible processes in volume V of the system:

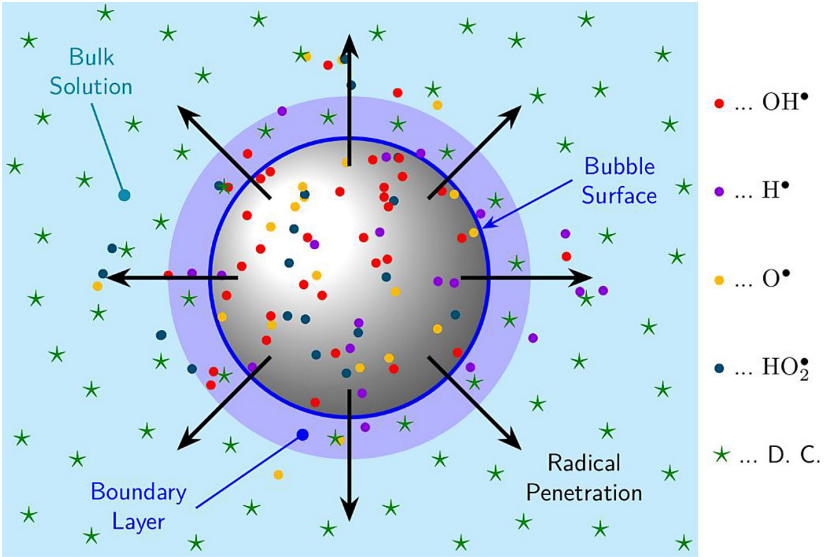

Figure 1. Schematic of radical production and penetration in a single cavitation bubble, "D. C." stands for dissolved compounds. Figure created by the author, inspired by a schematic presented in a study by Peng et al. (2022)

$$\mathcal{P} = \int_V \sum_{\alpha=1}^{N} J^{(\alpha)} X^{(\alpha)} \, \mathrm{d}V \tag{2}$$

In this case, the superscripts do not denote exponentiation or a derivative but rather serve as summation indices. For small deviations from equilibrium, a linear relationship exists between generalized thermodynamic fluxes and forces:

$$J^{(\alpha)} = L^{(\alpha\alpha)} X^{(\alpha)} \tag{3}$$

where: L is the so-called phenomenological coefficient.

For a given irreversible process α, the corresponding flux $J^{(\alpha)}$ and force $X^{(\alpha)}$ must be of the same tensorial order. Among the considered irreversible processes, shear fluid flow can be described by second-order tensors, electromagnetic quantities by vectors (first-order tensors), and chemical reactions by scalar quantities (Demirel, 2014; de Groot and Mazur, 1984; Maršík, 1999).

Curie–Prigogine principle

This fundamental principle (Prigogine, 1967) states that in an isotropic medium, where physical properties behave uniformly in all spatial directions, only irreversible processes characterized by thermodynamic quantities of the same tensorial order may interact. This can generally be expressed as:

$$J_{kl}^{(p)} = L^{(pp)} X_{kl}^{(p)}, \quad \forall p = 1,2,\dots,P; \tag{4}$$

$$J_{m}^{(r)} = L^{(rr)} X_{m}^{(r)}, \quad \forall r = 1,2,\dots,R; \tag{5}$$

$$J^{(s)} = L^{(ss)} X^{(s)}, \quad \forall s = 1,2,\dots,S; \tag{6}$$

where: indices $k, l, m = 1, 2, 3$ represent summation indices in Einstein notation, indicating the tensorial order of the quantities involved.

The upper indices p, r, s denote all irreversible processes in an isotropic system and thus the final number of required P Equations 4, 5, and 6. In total, there are second-order, R first-order, and S zero-order tensors representing thermodynamic fluxes and forces describing every irreversible process possible (Fialová and Pochylý, 2021; de Groot and Mazur, 1984; Prigogine, 1967).

Consequently, processes involving the magnetic field (vector quantities) and chemical reactions (scalar quantities) cannot directly influence one another in an isotropic medium. The Curie–Prigogine principle implies that the medium (in this case, wastewater) must exhibit anisotropy to enable interaction between these two irreversible processes. Anisotropy of fluids can be achieved through hydrodynamic cavitation, which inherently generates free radicals. The introduction of an external magnetic field can further enhance the production of these radicals, improving the overall degradation efficiency of wastewater treatment. In this case, the coupled relationships between irreversible processes can be written in matrix form. The following matrix represents the symbolic block structure of phenomenological coefficients coupling tensorial quantities of different orders:

$$\begin{bmatrix} J_{ij}^{(p)} \\ J_{m}^{(r)} \\ J^{(s)} \end{bmatrix} = \begin{bmatrix} L_{ijkl}^{(pp)} & L_{ijn}^{(pr)} & L_{ij}^{(ps)} \\ L_{mkl}^{(rp)} & L_{mn}^{(rr)} & L_{m}^{(rs)} \\ L_{kl}^{(sp)} & L_{n}^{(sr)} & L^{(ss)} \end{bmatrix} \cdot \begin{bmatrix} X_{kl}^{(p)} \\ X_{n}^{(r)} \\ X^{(s)} \end{bmatrix} \tag{7}$$

for $i, j, k, l, m, n = 1, 2, 3$ in a three-dimensional problem (Demirel, 2014; Fialová and Pochylý, 2021).

Applying the theory in wastewater treatment

Let us now restrict our consideration to a set of three irreversible processes relevant to the investigated problem: the influence of a magnetic field (index 1), compressible fluid flow (index 2), and chemical reactions (index 3). All interactions between respective fluxes and forces are governed by phenomenological coefficients L , which include so-called coupling coefficients – i.e., off-diagonal elements in the phenomenological matrix, where the upper indices differ. This simplified case can be generally expressed as:

$$\begin{bmatrix} J_{i}^{(1)} \\ J^{(2)} \\ J^{(3)} \end{bmatrix} = \begin{bmatrix} L_{ij}^{(11)} & L_{i}^{(12)} & L_{i}^{(13)} \\ L_{j}^{(21)} & L^{(22)} & L^{(23)} \\ L_{j}^{(31)} & L^{(32)} & L^{(33)} \end{bmatrix} \cdot \begin{bmatrix} X_{j}^{(1)} \\ X^{(2)} \\ X^{(3)} \end{bmatrix} \tag{8}$$

The current objective is the experimental evaluation of the individual contributions of thermodynamic forces X to the resulting fluxes J, as expressed through the corresponding phenomenological coefficients L. However, the potential symmetry of the coupling coefficients has

not yet been addressed. Onsager reciprocity relations play a significant practical role in linear non-equilibrium thermodynamics, as they allow for a substantial reduction in the number of phenomenological coefficients – and consequently, in the number of independent experimental methods required to determine them – by nearly half. This is because, according to Onsager, the coefficient matrix $L^{(\alpha\beta)}$ in Equation 8 must be either symmetric or antisymmetric, which can be mathematically expressed as $L^{(\alpha\beta)} = \pm L^{(\beta\alpha)}$ (de Groot and Mazur, 1984; Pokrovskii, 2013).

Substituting the relevant physical quantities into expression (8) gives:

$$\begin{bmatrix} M_i \\ \frac{1}{3}\Pi_{kk} \\ J \end{bmatrix} = -\frac{1}{T}\begin{bmatrix} L_{ij}^{(11)} & L_i^{(12)} & L_i^{(13)} \\ L_j^{(21)} & L^{(22)} & L^{(23)} \\ L_j^{(31)} & L^{(32)} & L^{(33)} \end{bmatrix} \cdot \begin{bmatrix} H_j \\ v_{kk} \\ A \end{bmatrix} \quad (9)$$

The thermodynamic system temperature is indicated by T, $M_{i\ Z}$denotes the magnetization vector of the medium, H_j is the magnetic field strength vector, $\frac{1}{3}\Pi_{kk}$ represents the spherical part of the viscous stress tensor (Π_{ij}), v_{kk} corresponds to the divergence of the velocity vector field v_k, and the scalar quantities J and A denote the chemical reaction rate and chemical affinity, respectively. The phenomenological coefficient $L_{ij}^{(11)}$ is associated with magnetic susceptibility X_m, while $L^{(22)}$ corresponds to the bulk viscosity b and $L^{(33)}$ defines the chemical affinity coefficient. Consequently, chemical reaction rate is defined by three terms representing the magnitude of contribution from each of the considered irreversible processes:

$$J = -\frac{L_j^{(31)}}{T}H_j - \frac{L^{(32)}}{T}\frac{\partial v_k}{\partial x_k} - \frac{L^{(33)}}{T}A \quad (10)$$

The divergence of velocity in Eq. (10) can be expressed from the continuity equation. Assuming a barotropic fluid, where density ρ depends solely on pressure (any changes with temperature are neglected), the relationship between density and pressure p can be expressed using the definition of bulk modulus and speed of sound c in the fluid. This approach yields the substitution for velocity divergence as follows:

$$\frac{\partial v_k}{\partial x_k} = -\frac{1}{\rho c^2}\frac{\mathrm{d}p}{\mathrm{d}t} \quad (11)$$

Since pressure is a more convenient quantity to measure than flow velocity, the substitution (11) can be introduced into the expression (10) to produce the final formula for the chemical reaction rate:

$$J = -\frac{L_j^{(31)}}{T}H_j - \frac{L^{(32)}}{T\rho c^2}\frac{\mathrm{d}p}{\mathrm{d}t} - \frac{L^{(33)}}{T}A \quad (12)$$

The expression (12) highlights the dependence of the thermodynamic flux J on quantities of different physical nature. It is not solely a function of chemical affinity; the intensity of the applied magnetic field and the substantial unsteady variations in pressure induced by HC also play a major role. It also clearly indicates which quantities need to be monitored and measured during the experiment. In an effort to further generalize the developed mathematical model, other irreversible processes could be incorporated in the future, such as different types of diffusion-based mechanisms, heat transfer and other thermal effects, viscous fluid flow, etc. (Demirel, 2014; Fialová and Pochylý, 2021; de Groot and Mazur, 1984; Kundu, 2008).

EXPERIMENTAL SETUP

The hydrodynamic cavitation reactor (HCR) was used for this experiment. It consists of a Venturi nozzle, a magnetic circuit, a piping system with two ball valves and a bypass option (as shown in Figure 2 and 3), an eight-liter tank equipped with a three-way valve to induce vacuum or overpressure within the system, and measurement instrumentation (pressure, flow rate, and temperature sensors). The experimental setup is also equipped with two centrifugal pumps in series (Calpeda S.p.A., Italy) with a power output of 0.33 kW, ensuring the required flow of the treated water through the piping system. The impellers of these pumps are made of stainless steel, which prevents any contamination of the treated water.

Component specifications

The Venturi nozzle induces hydrodynamic cavitation by locally reducing the flow cross section, where the increased flow velocity leads to a pressure drop down to the saturated vapor pressure. The internal diameter of the nozzle is 5.8 mm, narrowing to 2.7 mm at the throat (Figure 3).

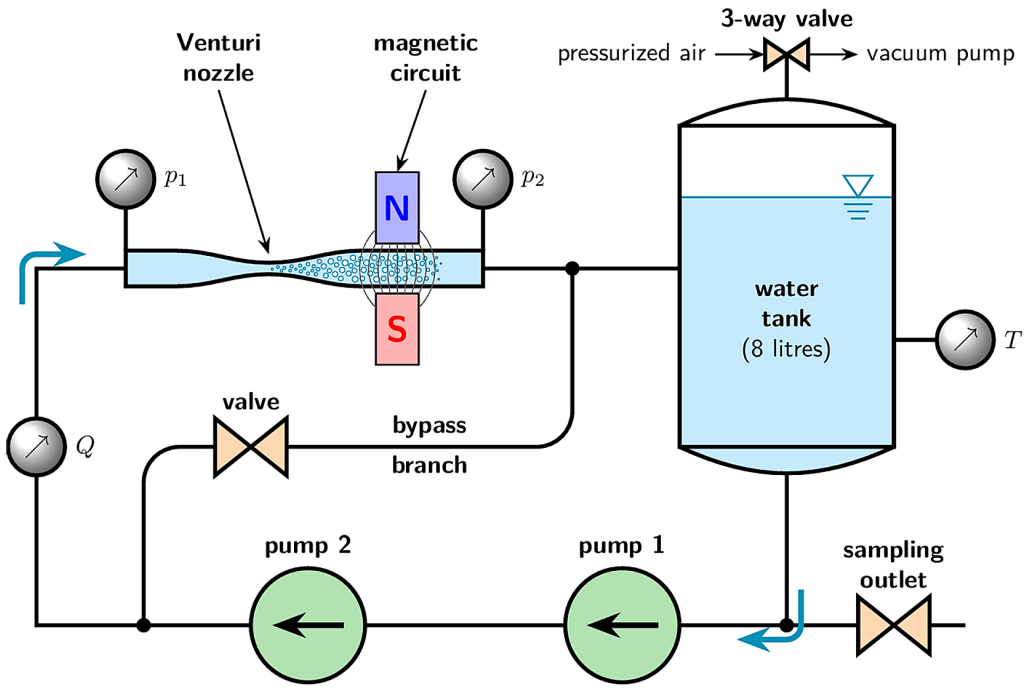

Figure 2. Schematic of the experimental setup

The magnetic circuit provides an external magnetic field with a flux density of approximately 0.65 Tesla. A key advantage in the context of energy sustainability is that supplying an external magnetic field would not lead to an increase in operational costs of the previously validated and patented CaviPlasma technology by Marsalek et al., 2020 (a synergistic combination of HC and low-temperature plasma discharge). To preserve the low energy demands of this treatment process, the current study prioritized the use of permanent neodymium magnets coupled with metal extensions. The circuit is arranged in a specific configuration which directs and concentrates the magnetic field to a specific region within the Venturi nozzle and applies it perpendicularly to the flow direction. Three configurations were studied:

- Placing the magnetic circuit at the site of cavitation inception (near the nozzle throat).
- Placing the magnetic circuit at the site of cavitation cloud collapse.
- Absence of magnetic field (HC only).

To monitor real-time values of the above-mentioned parameters, the experimental circuit includes an inductive flow meter, a resistance thermometer, and two pressure gauges positioned upstream and downstream of the Venturi nozzle. Table 1 summarizes the specifications of the listed sensors, including the measurement range of the respective quantity.

Parameter regulation

There are three main options for regulating the intensity of cavitation within the experimental setup. The first degree of freedom is the variable flow rate, which is controlled by operating the centrifugal pumps in different configurations. In the absence of a frequency inverter for adjusting the pump speed, only two operational modes can be distinguished: running either one or both pumps simultaneously. Additionally, the flow rate can be indirectly adjusted by opening the ball valve located in the bypass branch (see Figure 2).

The second parameter involves the adjustment of the pressure within the experimental setup (relative to atmospheric pressure), which has by far the greatest impact on the cavitation intensity (Lei et al., 2024). Figure 2 illustrates the possibility of connecting either a compressor or a vacuum pump to the water tank. The maximum achievable values of overpressure and vacuum are limited by the pipe sealing and the measurement range of the pressure sensors used (see Table 1).

In order to enhance the potential interaction of irreversible processes under experimental conditions, the magnetic circuit surrounding the cavitation nozzle must be positioned optimally with

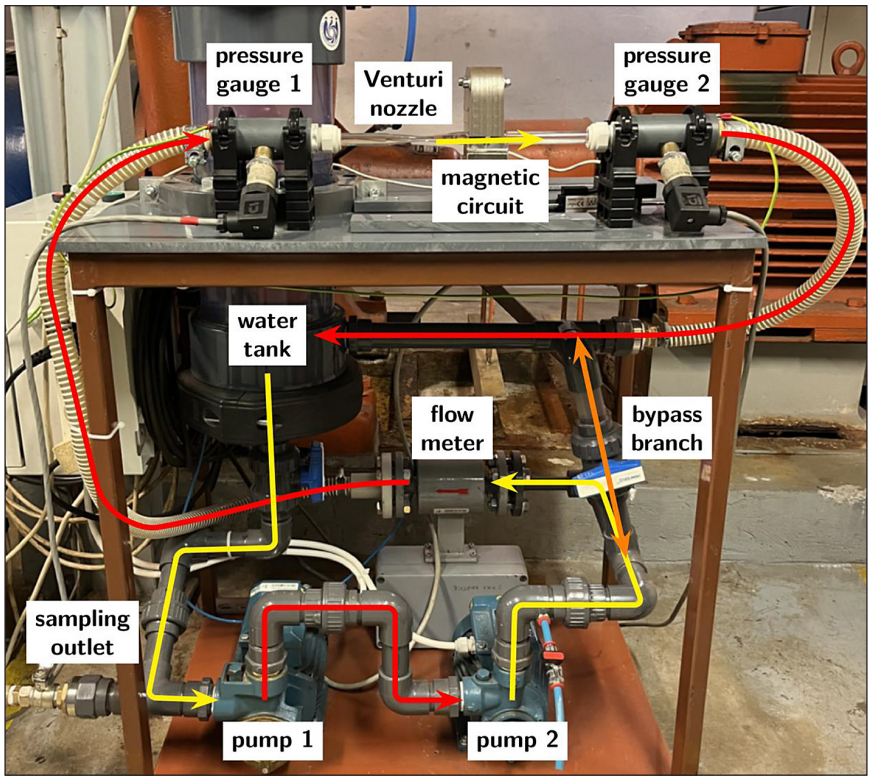

Figure 3. Image of the experimental setup

Table 1. Physical measurement sensors and their specifications

Sensor	Manufacturer and/or type	Parameter range
Pressure sensor	BD Sensors (DMP 331)	0 to 400 kPa
Inductive flow meter	Kompakt (TCM 142/93)	0.612 to 6.12 m^3/h
Resistance thermometer	Pt100 Type A	-70 to +300 °C

respect to the cavitation zone. To ensure greater flexibility, a sliding mechanism allows for axial adjustment of the magnetic circuit along the Venturi nozzle. When both pumps are in operation, the cavitation zone extends downstream into the pipe section beyond the nozzle (supercavitation may occur). The cavitation region can be reduced to the desired position by pressurizing the loop using a compressor. Alternatively, when only one of the pumps is in operation, the formation of cavitation needs to be supported by inducing a vacuum in the system via the vacuum pump.

Chemical analysis

Since the phenomenological coefficients from Equation 12 are determined experimentally, it is necessary to obtain information about the chemical changes in the treated wastewater. From a chemical perspective, several parameters can be evaluated to indicate the presence of ROS, such as hydroxyl radicals, hydrogen peroxide, ozone, and similar compounds. To capture the widest possible range of chemical indicators, measurements included not only the concentration of hydrogen peroxide and ozone but also the TDS parameter. In addition, pH, ORP, alkalinity, and salinity were assessed, as ORP in particular may indicate the presence of free radicals, even after they have reacted.

A waterproof PC 6 tester (XS Instruments, Italy) was utilized for the measurement of pH, ORP, conductivity, TDS, and salinity. This tester is equipped with a replaceable sensor and an automatic temperature compensation function. The ORP is a parameter describing the working electrode potential E measured in millivolts with respect to the reference electrode potential. The oxidation-reduction reactions occurring in an electrochemical cell (containing both cathode and

anode, along with the electrolyte) between oxidants (Ox) and reductants (Red) can be generally expressed as (Matsumoto et al., 2022):

$$\mathrm{Ox} + n\,e^- \rightleftharpoons \mathrm{Red} \tag{13}$$

where: n is the number of electrons (e^-) transferred.

While this param eter can be measured using a potentiometer, the calculation of E is governed by the so-called half-cell Nernst equation (Matsumoto et al., 2022):

$$E = E^\circ - \frac{RT}{nF} ln\left(\frac{a_{\mathrm{Red}}}{a_{\mathrm{Ox}}}\right) \tag{14}$$

where: E° corresponds to the standard hydrogen electrode (SHE) potential for the redox couple under standard conditions, R and F represent the gas constant and Faraday constant, respectively, and the absolute temperature is indicated by T.

Quantities $\alpha_{\mathrm{Red}}$and α_{Ox} are the equilibrium activities (effective concentrations) of the reduced and oxidized forms. Their ratio, as expressed in (14), is generally defined as products over reactants and can also be denoted as the reaction quotient, Q_r. The Nernst equation in the form (14) describes a half-cell reaction, where the chemical Equation 13 is written in the reduction direction (Matsumoto et al., 2022).

This study also employed a modified titanyl method of H_2O_2 determination (Eisenberg, 1943; Lukes et al., 2014; Marsalek et al., 2020), utilizing the reaction of peroxide with titanyl ions to form a yellow-colored pertitanic acid complex to measure peroxide concentration:

$$\mathrm{Ti^{4+}} + \mathrm{H_2O_2} + 2\,\mathrm{H_2O} \longrightarrow \longrightarrow \mathrm{TiO_2 \cdot H_2O_2} + 4\,\mathrm{H^+} \tag{15}$$

Absorbance was measured spectrophotometrically on a Spark® Multimode Microplate Reader (Tecan Austria GmbH). The measurement of acid capacity was conducted using a titrimetric test kit Visocolor® HE Alkalinity AL 7 (Macherey-Nagel GmbH & Co.KG, Germany). The specifications of the above-mentioned instruments are summarized in Table 2.

Methodology

Tap water was used for this measurement and was collected into an open container at least 24 hours prior to the experiment to facilitate the outgassing of volatile compounds, primarily chlorine. This step was necessary, as the presence of these chemicals could negatively affect the chemical analysis. Tap water was preferred over other options because it exhibits long-term stability in its chemical properties (such as mineral concentration, pH, etc.), which allows for maximizing the consistency of initial conditions in each measurement. Before the experiment was initiated, a "sample 0" was collected to analyze the default values of all described chemical parameters.

Once the pumps are activated, the properties of the water are immediately chemically altered by hydrodynamic cavitation. Such "contaminated" water cannot be reused in subsequent measurements and has to be replaced. To ensure the integrity of the experimental loop before each subsequent measurement, demineralized water

Table 2. Sensor and instrument specifications for chemical analysis

XS Tester PC 6 – KIT		
Quantity	Parameter accuracy	Parameter range
pH	±0.01	-2 to 16
ORP	–	-1000 to +1000 mV
TDS	±2% of full scale	0.01 ppm to 199.9 ppt
Conductivity	±2% of full scale	0.01 µS to 199.9 mS
Salinity	–	0.01 mg/L to 100 g/L
Spark® Multimode Microplate Reader		
Quantity	Parameter accuracy	Parameter range
Wavelength	≤ 0.8 nm	200 to 1000 nm
Visocolor® HE Alkalinity AL 7		
Quantity	Parameter accuracy	Parameter range
Alkalinity	≤ 0.2 mmol/L	0 to 7.2 mmol/L

was used for the flushing process. Based on the estimated volume of water in the test loop and the average flow rate, the duration of a single cycle – defined as the time required for all the water in the tank to pass through the nozzle at least once – was calculated. The total volume of the test circuit was estimated at 8 liters, although the loop was filled to only 6 liters.

To ensure that the cavitation region remained confined within the Venturi nozzle, the vacuum pump option was employed during the operation of a single pump to achieve and maintain the optimal cavitation intensity. During the initial measurements, continuous pump operation led to rapid heating of the relatively small volume of treated water in the system. Therefore, passive cooling of the experimental loop was subsequently implemented to preserve the initial conditions.

To analyze the correlation between the number of cycles and the chemical parameters, the remaining samples were collected after a set number of full cycles: 1, 2, 4, 8, and 16. According to the data from the flow meter, the average flow rate during the simultaneous operation of both pumps was determined to be Q = 0.2 L/s, suggesting that one cycle lasts approximately 30 seconds. Based on this, a sampling schedule was established and is shown in Table 3. The chemical analysis of the collected water samples was carried out at the Institute of Botany of the Czech Academy of Sciences.

RESULTS AND DISCUSSION

Of all the measured chemical parameters, the most significant changes were observed in the pH and ORP of the treated water samples (as shown in Figure 4 and 5). The noticeable differences between the initial measured values are primarily attributed to the fact that rapid changes in the chemical properties of the treated water occur mainly at the very beginning of the experiment. The first samples were then collected 30 seconds after the start of the experiment (see Table 3), which provides sufficient time for such variations to develop.

Table 3. Sampling schedule

Sample	Cycles	Seconds	Elapsed time
1	1	30 s	0:30
2	2	30 s	1:00
3	4	60 s	2:00
4	8	120 s	4:00
5	16	240 s	8:00

Changes in the remaining parameters were mostly measured below the detection limit (hydrogen peroxide, ozone) or showed no significant variation under the influence of the external magnetic field. The alkalinity of the samples did not change significantly with the increasing number of cycles, with an average value ranging between 2.6 and 2.8 mmol/L. The same applies to salinity (~195 mg/L), conductivity (~410 µS/cm), TDS (~290 ppm), and water hardness (>7 °d).

Based on the thermometer data, the average saturation vapor pressure value was determined, and the cavitation number σ was calculated according to Equation 1, yielding a stable value of ~1.28 with 200 mbar below the atmospheric pressure in the system. At higher σ values, the cavitation region would become unstable, while at lower values, it extended into the pipeline system downstream of the Venturi nozzle. Both options are considered undesirable due to difficulties in proper positioning of the magnetic circuit.

Changes in pH values

While pH values (see Figure 4) remained constant (pH ≈ 7.7) with an increasing number of cycles in the absence of the magnetic circuit, a gradual increase was observed in both cases involving the influence of an external magnetic field. When the magnetic circuit was placed in the region of the cavitation cloud collapse, the pH increased more steeply at first and then stabilized at approximately pH = 7.85 with the increasing number of cycles. In contrast, when the magnetic field was applied directly at the site of HC formation (near the throat of the Venturi nozzle), the measured pH values were generally higher, although the increase was more gradual. The maximum recorded value was pH = 8.07, and the trend suggests a continued rise with further cycles.

According to studies (Boczkaj and Fernandes, 2017; Hübner et al., 2024; Rajoriya et al., 2016; Rayaroth et al., 2023), however, the reaction of ROS with organic pollutants should lead to a gradual decrease in pH. These reactions are typically multi-step, and their products usually include carboxylic acids and CO_2. This results in the release of H^+ ions into the solution,

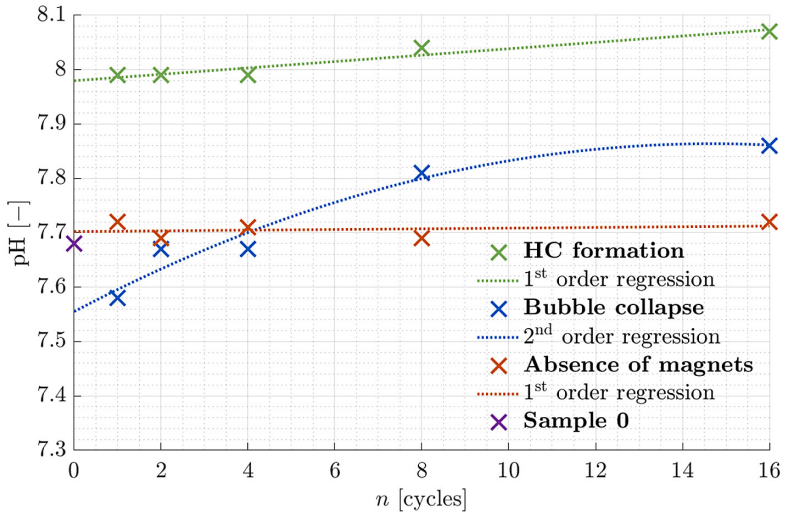

Figure 4. Dependence of sample pH on the number of cycles

effectively lowering the pH value. Residual hydrogen peroxide may also act as a weak acid, although its effect depends on other conditions and the composition of the treated wastewater. This discrepancy can be explained by the use of clean tap water containing few reactive components. As a result, ROS have few organic pollutants to oxidize and instead react with dissolved inorganic substances, water molecules, or with each other, leading to the release of OH^- ions that increase the overall pH. Tap water may also contain bicarbonates (HCO_3^-), which react with hydroxyl radicals and further shift the pH value toward more alkaline values. In addition, this process is closely related to the release of dissolved gases (including CO_2) during HC, which normally contributes to the slightly acidic nature of the solution (Kalmár et al., 2020)

Changes in ORP

In the evaluation of redox potential (see Figure 5), a clear influence of the magnetic field on this parameter is again visible. During treatment with pure HC, the measured ORP values remained essentially constant regardless of the number of cycles. The magnetic field appears to cause a rapid increase in ORP at the beginning of the experiment, followed by a gradual decline and stabilization with additional cycles. Although this parameter does not directly indicate the concentration of free radicals, it reflects their presence. Since hydroxyl radicals are extremely reactive oxidants with a redox potential of up to +2.8 V (Satyam and Patra, 2025; Zupanc et al., 2013), their production leads to a temporary increase in ORP. Upon reacting with target compounds (OH• extracts electrons or hydrogen atoms from the compound), the radical is reduced, forming water or hydroxide ions. After these reactions take place, the ORP decreases and stabilizes at a new equilibrium value, which may differ from the original. In contrast to pH, ORP data thus provides clear evidence for the presence of hydroxyl radicals during the treatment of water with the combined effect of hydrodynamic cavitation and an external magnetic field. It should be noted that this effect is more pronounced when the magnetic circuit is placed in the region of cavitation cloud collapse.

When retrospectively reflecting on the obtained data (see Figures 4 and 5) in light of the derived Equation 12, a clear change in chemical reaction rate J was observed. The presence (or absence) of the first term in Equation 12, which describes the influence of the magnetic field, demonstrably affects the production of ROS (mainly free radicals). However, the applied methodology currently does not allow for quantifying the individual contribution of each irreversible process.

Given the conditions induced by HC – namely, an anisotropic and heterogeneous environment – the magnetic field influences the chemical potentials present in the water volume by altering Helmholtz free energy. This effect manifests in both tap and polluted water, as both contain a substantial amount of dissolved elements. These substances are subjected to significant pressure fluctuations (second term in Equation 12 and

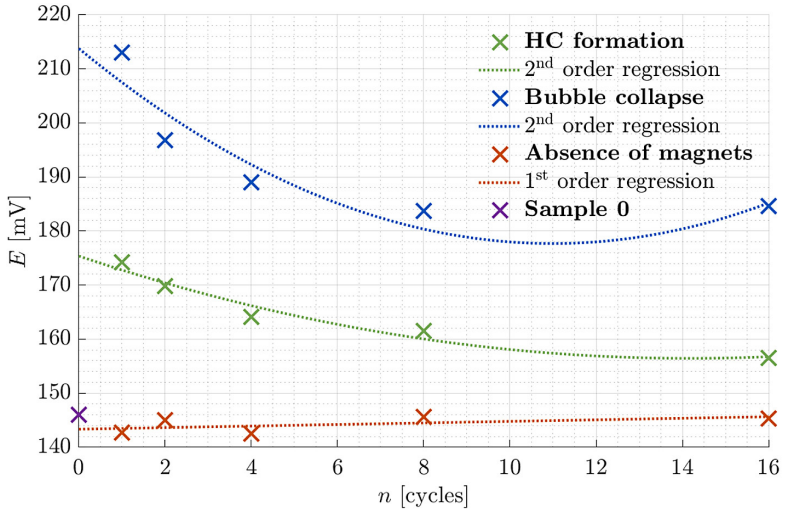

Figure 5. Dependence of sample ORP on the number of cycles

temperature changes, which increase the chemical potentials and their affinity toward chemical reactions (third term in Equation 12).

While the first and second terms of Equation 12 are relevant only during the experiment, the third term determines the sustainability and stability of the treatment process after the pumps are shut down. Chemical potentials altered by the aforementioned effects remain within the liquid volume even after the process is finished. Depending on the composition of substances dissolved in the treated water, the cleaning effect can either be enhanced or suppressed. In this case, the results of the conducted experiment clearly demonstrate that the presence of an external magnetic field of sufficient strength induced desirable chemical changes in a cavitating liquid, particularly in the context of wastewater treatment. Therefore, the proposed hypothesis can be considered experimentally validated.

Among the evaluated chemical parameters (pH, ORP, TDS, salinity, alkalinity, and concentrations of H_2O_2 and O_3), the most significant changes were observed in pH and redox potential. The sharp increase followed by a gradual decline in ORP suggests enhanced production of free radicals, primarily OH•. Subsequently, hydroxyl radicals undergo non-selective chemical reactions, either with organic pollutants, water molecules, or with each other to form less reactive ROS (typically H_2O_2) through recombination reactions. An increased concentration of hydro gen peroxide was, however, not detected, which may indicate that an optimal configuration of radical production was achieved. In that case, the majority of hydroxyl radicals generated during the cavitation bubble collapse possessed sufficient penetration depth to react directly with organic contaminants.

The observed increase in pH from neutral to alkaline values, on the other hand, contradicted initial expectations. This may be attributed to the use of tap water, which contains minimal concentrations of organic pollutants, but also provides stable initial conditions for the conducted experiments. While the oxidation of organic pollutants leads to the production of acidic byproducts and a decrease in pH, alternative reduction-oxidation reactions likely took place instead, resulting in an overall increase in pH.

Future technology

Follow-up experiments should, therefore, focus on evaluating treatment efficiency for different wastewater types, such as industrial effluents or even river water (used by Hordieiev et al. (2024). If detectable changes in H_2O_2 concentration are observed under such conditions, this would further support the beneficial impact of the magnetic field on the AOP enhancement. In this context, a more comprehensive approach to detecting the presence of free radicals should also be adopted – ideally using a direct detection method such as spin trapping with the use of electron paramagnetic resonance (EPR). At the same time, maintaining a balance between radical production and their effective penetration depth remains critical.

For potential scale-up of this technology, attention must also be paid to achieving sufficient magnetic field strength in larger volumes of treated wastewater. The use of permanent magnets, as applied in the current study, suffers from a rapid loss of field strength with increasing distance from the magnetic assembly due to field dissipation. As a logical next step in intensifying the treatment process, the use of electromagnets should be considered. Unlike permanent magnets, electromagnets offer the advantage of tunable output parameters controlled by the input voltage. However, their drawback in this context is obvious – the energy self-sufficiency achievable with permanent magnets cannot be maintained when electromagnets are used.

Given that hydrodynamic cavitation reactors are most commonly combined synergistically with low-temperature plasma, it is also worth considering the integration of both technologies with the influence of a magnetic field. A subsequent comparison of their individual contributions to ROS production could reveal the optimal configuration for developing a combined technology.

CONCLUSIONS

The novel application of non-equilibrium thermodynamics provided a framework for evaluating water purification processes through interrelations between variables of different physical nature. By incorporating the Curie–Prigogine principle and Onsager reciprocity relations, it was possible to mathematically describe the influence of relevant physical phenomena on the initiation and progression of chemical reactions within the volume of the treated liquid. This qualitative approach, grounded in the concept of entropy production, not only enabled a more purposeful experimental design but also allowed for informed predictions of the outcomes.

As this study represents a pilot experiment in this field, the current dataset is not yet sufficient to allow for a robust statistical evaluation of the results, such as the calculation of standard deviations, confidence intervals, or uncertainties. However, the experimental framework has been designed with repeatability in mind, and the promising preliminary findings will serve as the basis for subsequent series of measurements under varied conditions.

Acknowledgements

This work was supported by the Czech Science Foundation (GAČR) under Grant Agreement No. GA22-11456S.

REFERENCES

1. Abramov, V., Abramova, A., Bayazitov, V., Kameneva, S., Veselova, V., Kozlov, D., Sozarukova, M., Baranchikov, A., Fedulov, I., Nikonov, R., Cravotto, G., (2022). Fast degradation of tetracycline and ciprofloxacin in municipal water under hydrodynamic cavitation/plasma with CeO_2 nanocatalyst. *Processes 10*. https://www.mdpi.com/2227-9 717/10/10/2063, https://doi.org/10.3390/pr10102063
2. Abramov, V.O., Abramova, A.V., Cravotto, G., Nikonov, R.V., Fedulov, I.S., Ivanov, V.K., (2021). Flow-mode water treatment under simultaneous hydrodynamic cavitation and plasma. Ultrasonics Sonochemistry 70, 105323. https://www.sciencedirect.com/science/article/ pii/S135041772030777X, https://doi.org/10.1016/j.ultsonch.2020.105323
3. Boczkaj, G., Fernandes, A., (2017). Wastewater treatment by means of advanced oxidation processes at basic pH conditions: A review. *Chemical Engineering Journal 320*. https://doi.org/10.1016/j.cej.2017.03.084
4. Cai, R., Yang, H., He, J., Zhu, W., (2009). The effects of magnetic fields on water molecular hydrogen bonds. *Journal of Molecular Structure 938*, 15–19. https:// www.sciencedirect.com/science/article/pii/S0022286009005559, https://doi.org/10.1016/j.molstruc.2009.08.037
5. Chang, K.T., Weng, C.I., (2006). The effect of an external magnetic field on the structure of liquid water using molecular dynamics simulation. *Journal of Applied Physics 100*, 043917. https://doi.org/10.1063/1.2335971
6. Demirel, Y., (2014). *Nonequilibrium Thermodynamics: Transport and Rate Processes in Physical, Chemical and Biological Systems: Third Edition. 3rd ed.*, Elsevier, Amsterdam, The Netherlands.
7. Dixit, D., Thanekar, P., Bhandari, V.M., (2023). Enhanced degradation of metformin using surface-coated vortex diodes. *Chemical Engineering and Processing - Process Intensification 193*, 109572. https://www.sciencedirect.com/science/article/pii/S0255270123003094, https://doi.org/10.1016/j.cep.2023.109572
8. Eisenberg, G., (1943). Colorimetric determination of hydrogen peroxide. *Industrial & engineering chemistry. Analytical edition 15*, 327–328.
9. Fialová, S., Pochylý, F., (2021). Constitutive equations for magnetic active liquids. *Symmetry 13.*

https://www.mdpi.com/2073-8994/13/10/1910, https://doi.org/10.3390/ sym13101910

10. Filipić, A., Dobnik, D., Gutiérrez-Aguirre, I., Ravnikar, M., Košir, T., Špela Baebler, Štern, A., Žegura, B., Petkovšek, M., Dular, M., Mozetič, M., Zaplotnik, R., Primc, G., (2023). Cold plasma within a stable supercavitation bubble – a breakthrough technology for efficient inactivation of viruses in water. Environment International 182, 108285. https://www.sciencedirect.com/ science/article/pii/ S0160412023005585, https://doi.org/10.1016/j.envint.2023.108285
11. de Groot, S.R., Mazur, P., (1984). *Non-equilibrium Thermodynamics*. Unabridged, corrected dover edition; first published ed., Dover Publications, New York.
12. Gągol, M., Przyjazny, A., Boczkaj, G., (2018). Wastewater treatment by means of advanced oxidation processes based on cavitation– a review. *Chemical Engineering Journal 338*, 599–627. https://www.sciencedirect.com/science/article/pii/S138589471830055X, https:// doi.org/10.1016/j.cej.2018.01.049
13. Hordieiev, A., Kalda, G., Pashechko, M., Hanzyuk, A., Tkachuk, V., Kostiuk, N., (2024). Study of the influence of cavitation and magnetic field on the change of water properties and its purification in a vibrating machine with determination of drive modes. *Advances in Science and Technology Research Journal 18*, 234–245. https://doi.org/10.12913/22998624/186545, https://doi.org/10.12913/22998624/186545
14. Hübner, U., Spahr, S., Lutze, H., Wieland, A., Rüting, S., Gernjak, W., Wenk, J., (2024). Advanced oxidation processes for water and wastewater treatment– guidance for systematic future research. *Heliyon 10*, e30402. https://www.sciencedirect.com/science/article/ pii/S2405844024064338, https://doi.org/10.1016/j.heliyon.2024.e30402
15. Kalmár, C., Klapcsik, K., Hegeduss, F., (2020). Relationship between the radial dynamics and the chemical production of a harmonically driven spherical bubble. *Ultrasonics Sonochemistry 64*, 104989. https://www.sciencedirect.com/science/article/pii/S1350417719309666, https://doi.org/10.1016/j.ultsonch.2020.104989
16. Kanthale, P., Pandey, R., Thakur, D., Gujar, S.K., Gogate, P.R., Thakre, S., Dutta, C., (2023). Application of combined hydrodynamic cavitation and fenton reagent for cod reduction of cellulosic fiber industry effluents. *Journal of Water Process Engineering 56*, 104500. https://www.sciencedirect.com/science/article/pii/S2214714423010206, https://doi.org/ 10.1016/j.jwpe.2023.104500
17. Kundu, P.K., 2008. *Fluid mechanics. 4th ed*., Academic Press, Burlington.
18. Lei, E., Yuan, X., Xiang, K., Shao, Z., Hong, F., Huang, Y., (2024). Research progress of hydrodynamic cavitation reactors in the field of water treatment: A review. *Journal of Water Process Engineering 66*, 105997. https://www.sciencedirect.com/science/article/pii/ S2214714424012297, https://doi.org/10.1016/j.jwpe.2024.105997.
19. Liu, B., Gao, B., Xu, X., Hong, W., Yue, Q., Wang, Y., Su, Y., 2011. The combined use of magnetic field and iron-based complex in advanced treatment of pulp and paper wastewater. *Chemical Engineering Journal 178*, 232–238. https://www.sciencedirect.com/science/ article/pii/S1385894711012976, https://doi.org/10.1016/j.cej.2011.10.058
20. Lukes, P., Dolezalova, E., Sisrova, I., Clupek, M., (2014). Aqueous-phase chemistry and bactericidal effects from an air discharge plasma in contact with water: evidence for the formation of peroxynitrite through a pseudo-second-order post-discharge reaction of H_2O_2 and HNO_2. *Plasma sources science & technology 23*.
21. Marsalek, B., Marsalkova, E., Odehnalova, K., Pochyly, F., Rudolf, P., Stahel, P., Rahel, J., Cech, J., Fialova, S., Zezulka, S., (2020). Removal of microcystis aeruginosa through the combined effect of plasma discharge and hydrodynamic cavitation. *Water 12*. https://www.mdpi.com/2073-4441/12/1/8, https://doi.org/10.3390/w12010008
22. Maršík, F., (1999). *Thermodynamics of Continua (In Czech). 1st ed.*, Academia, Prague, Czech Republic.
23. Matsumoto, K., Miyazaki, K., Hwang, J., Yamamoto, T., Sakuda, A., (2022). Electrode potentials part 1: Fundamentals and aqueous systems. *Electrochemistry 90*, 102001–102001. https://doi.org/10.5796/electrochemistry.22-66075
24. Nie, G., Hu, K., Ren, W., Zhou, P., Duan, X., Xiao, L., Wang, S., (2021). Mechanical agitation accelerated ultrasonication for wastewater treatment: Sustainable production of hydroxyl radicals. *Water Research 198*, 117124. https://www.sciencedirect.com/science/article/ pii/S0043135421003225, https://doi.org/10.1016/j.watres.2021.117124
25. Nie, S., Qin, T., Ji, H., Nie, S., Dai, Z., (2022). Synergistic effect of hydrodynamic cavitation and plasma oxidation for the degradation of rhodamine b dye wastewater. *Journal of Water Process Engineering 49*, 103022. https://www.sciencedirect.com/science/article/pii/S2214714422004664, https://doi.org/10.1016/j.jwpe.2022.103022
26. Lakshmi N.J., Gogate, P.R., Pandit, A.B., (2021). Treatment of acid violet 7 dye containing effluent using the hybrid approach based on hydrodynamic cavitation. *Process Safety and Environ mental Protection 153*, 178–191. https://www.sciencedirect.com/science/article/pii/S0957582021003645, https://doi.org/10.1016/j.psep.2021.07.023

27. Patil, P.B., Thanekar, P., Bhandari, V.M., (2022). Intensified hydrodynamic cavitation using vortex flow based cavitating device for degradation of ciprofloxacin. *Chemical Engineering Research and Design 187*, 623–632. https://www.sciencedirect.com/science/article/pii/S0263876222005263, https://doi.org/10.1016/j.cherd.2022.09.027
28. Peng, K., Tian, S., Zhang, Y., He, Q., Wang, Q., (2022). Penetration of hydroxyl radicals in the aqueous phase surrounding a cavitation bubble. *Ultrasonics Sonochemistry 91*, 106235. https://www.sciencedirect.com/science/article/pii/S1350417722003315, https://doi.org/10.1016/j.ultsonch.2022.106235.
29. Pokrovskii, V.N., (2013). A derivation of the main relations of nonequilibrium thermodynamics. *International Scholarly Research Notices 2013*, 906136. https://doi.org/10.1155/2013/906136
30. Prigogine, I., (1967). *Introduction to Thermodynamics of Irreversible Processes. 3rd ed.*, Interscience Publishers, a Division of John Wiley, New York.
31. Rajoriya, S., Carpenter, J., Saharan, V.K., Pandit, A.B., (2016). Hydrodynamic cavitation: an advanced oxidation process for the degradation of bio-refractory pollutants. *Reviews in Chemical Engineering 32*, 379–411. https://doi.org/10.1515/revce-2015-0075
32. Raut-Jadhav, S., Badve, M.P., Pinjari, D.V., Saini, D.R., Sonawane, S.H., Pandit, A.B., (2016). Treatment of the pesticide industry effluent using hydrodynamic cavitation and its combi nation with process intensifying additives (H_2O_2 and ozone). *Chemical Engineering Journal 295*, 326–335. https://www.sciencedirect.com/science/article/pii/S1385894716302492, https://doi.org/10.1016/j.cej.2016.03.019
33. Rayaroth, M.P., Boczkaj, G., Aubry, O., Aravind, U.K., Aravindakumar, C.T., (2023). Advanced oxidation processes for degradation of water pollutants – ambivalent impact of carbonate species: A review. Water 15. https://www.mdpi.com/2073-4441/15/8/1615, https://doi.org/10.3390/w15081615
34. Satyam, S., Patra, S., (2025). The evolving landscape of advanced oxidation processes in wastewater treatment: Challenges and recent innovations. Processes 13. https://www.mdpi.com/2227-9717/13/4/987, https://doi.org/10.3390/pr13040987
35. Thanekar, P., Garg, S., Gogate, P.R., (2020). Hybrid treatment strategies based on hydro dynamic cavitation, advanced oxidation processes, and aerobic oxidation for efficient removal of naproxen. *Industrial & Engineering Chemistry Research 59*, 4058–4070. https://doi.org/10.1021/acs.iecr.9b01395
36. Toledo, E.J., Ramalho, T.C., Magriotis, Z.M., (2008). Influence of magnetic field on physical–chemical properties of the liquid water: Insights from experimental and theoretical models. *Journal of Molecular Structure 888*, 409–415. https://www.sciencedirect.com/science/article/pii/S0022286008000434, https://doi.org/10.1016/j.molstruc.2008.01.010
37. Wang, Y., Wei, H., Li, Z., (2018). Effect of magnetic field on the physical properties of water. *Results in Physics 8*, 262–267. https://www.sciencedirect.com/science/article/pii/S2211379717317230, https://doi.org/10.1016/j.rinp.2017.12.022
38. Yi, L., Qin, J., Sun, H., Ruan, Y., Zhao, L., Xiong, Y., Wang, J., Fang, D., (2022). Improved hydrodynamic cavitation device with expanded orifice plate for effective chlorotetracycline degradation: Optimization of device and operation parameters. *Separation and Purification Technology 280*, 119840. https://www.sciencedirect.com/science/article/pii/S1383586621015471, https://doi.org/10.1016/j.seppur.2021.119840
39. Yoshimura, T., Watanabe, S., Ijiri, M., Ota, S., (2022). Development of processing technology using extremely high concentration cavitation energy by strong magnetic field. *Results in Materials 14*, 100289. https://www.sciencedirect.com/science/article/pii/S2590048X22000371, https://doi.org/10.1016/j.rinma.2022.100289
40. Zupanc, M., Kosjek, T., Petkovšek, M., Dular, M., Kompare, B., Širok, B., Željko Blaženka, Heath, E., (2013). Removal of pharmaceuticals from wastewater by biological processes, hydrodynamic cavitation and UV treatment. *Ultrasonics Sonochemistry 20*, 1104–1112. https://www.sciencedirect.com/science/article/pii/S1350417712002775, https://doi.org/10.1016/j.ultsonch.2012.12.003